Transparent Photo-Curable *co*-Polyacrylate/Silica Nanocomposites Prepared by Sol-Gel Process

Yen-Chun Chou, Yu-Young Wang, T.-E. Hsieh

Department of Materials Science and Engineering, National Chiao-Tung University, Hsinchu 30010, Taiwan, Republic of China

Received 7 July 2005; accepted 3 November 2006
DOI 10.1002/app.26228
Published online 3 May 2007 in Wiley InterScience (www.interscience.wiley.com).

ABSTRACT: This work prepared the highly transparent photo-curable *co*-polyacrylate/silica nanocomposites by using sol-gel process. The FTIR and ^{13}C NMR analyses indicated that during the sol-gel process, the hybrid precursors transform into composites containing nanometer-scale silica particles and crosslinked esters/anhydrides. Transmission electron microscopy (TEM) revealed that the silica particles within the average size of 11.5 nm uniformly distributed in the nanocomposite specimen containing about 10 wt % of Si. The nanocomposite specimens exhibited satisfactory thermal stability that they had 5% weight loss decomposition temperatures higher than 150°C and coefficient of thermal expansion (CTE) less than 35 ppm/°C. Analysis via derivative thermogravimetry (DTG) indicated that the crosslinked esters/anhydrides might influence the thermal stability of nanocomposite samples. The UV-visible spectroscopy indicated that the nanocomposite resins possess transmittance higher than 80% in visible light region. Permeability test revealed a higher moisture permeation resistance for nanocomposite samples, which indicated that the implantation of nano-scale silica particles in polymer matrix forms effective barrier to moisture penetration. Adhesion test of nanocomposite samples on glass substrate showed at least twofold improvement of adhesion strength compared with oligomer. This evidenced that the silica and the hydrophilic segments in nanocomposite resins might form interchains hydrogen bonds with the —OH groups on the surface of glass so the substantial enhancement of adhesion strength could be achieved. © 2007 Wiley Periodicals, Inc. J Appl Polym Sci 105: 2073–2082, 2007

Key words: nanocomposites; sol-gel process; silica; photo-curable; OLED encapsulation

INTRODUCTION

Because of the advantages such as low power consumption, high efficiency, wide viewing angle, short response time, and compact/lightweight nature of devices, organic light-emitting devices (OLEDs) have become one of the major flat-panel display technologies in recent years. However, the realization of OLEDs must overcome several difficulties such as the lifetime of light-emitting materials,[1] device structures,[2] and the need of encapsulation with extremely low H_2O/O_2 permeability.[3,4] To achieve a reliable OLED packaging by direct encapsulation, the resin with low curing temperature, short curing time, and low moisture/oxygen permeability is required. Photo-curable nanocomposites hence become one of feasible materials for such an application.

Organic–inorganic composites based on polymers have been widely investigated and they have many practical applications due to their unique physical and chemical properties. For examples, adding the nano-sized inorganic components into polymer matrices could improve the mechanical properties[5–8] and permeability[9,10] of polymers. One of the processing methods to add the inorganic fillers into polymers, the *in situ* sol-gel process, has been widely studied due to its high chemical uniformity, high purity, and good reproducibility. Starting from a homogeneous solution, sol-gel process provides better control over the microstructure and size of the inorganic fillers and has been adopted to prepare nano-particles[11,12] and organically modified silica[13,14] in polymers. For instance, Landry et al. had systematically reported the morphology, dynamic mechanical properties, and chemical analyses of PMMA/silica nanocomposite prepared by *in situ* sol-gel process.[15,16] However, most nanocomposites prepared via sol-gel process were thermally cured; relatively few reports were related to the photo-curable nanocomposites. Recently, photo-curable nanocomposite polymers have attracted a lot of research interests due to their versatile applications.[17,18]

This work reported the preparation and characterization of photo-curable *co*-polyacrylate composite resins containing nano-scale silica particles via sol-gel process. In contrast to the conventional sol-gel process

Correspondence to: T.-E. Hsieh (tehsieh@cc.nctu.edu.tw).
Contract grant sponsor: Ministry of Education of the Republic of China; contract grant number: 91-E-FA04-2-4.

Journal of Applied Polymer Science, Vol. 105, 2073–2082 (2007)

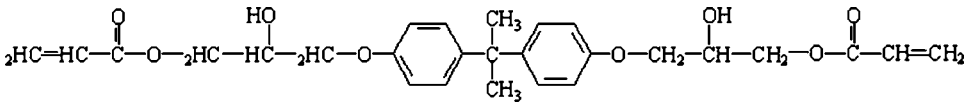

Figure 1 Chemical structure of bisphenol A epoxy diacrylate.

utilizing liquid water, ambient moisture was adopted in this work to hydrolyze precursors so as to confine the sizes of silica particles to nanometer scale and to avoid water molecules residing in composites. To comprehend the influences of moisture on other two ingredients in sol-gel reaction, the effects of acrylic acid/tetraethyl orthosilicate (TEOS) ratio on material properties were investigated in detail. Interactive relationships between TEOS/acrylic acid/moisture were explored to interpret the experimental results. Nanocomposite resins developed in this work were also applied to the direct encapsulation of OLEDs.[19] Related study indicated that higher adhesion strength and lower moisture permeability provided by the nanocomposite resins contribute to the better device performance and lifetime of encapsulated OLEDs.

EXPERIMENTAL

Materials

The oligomer, bisphenol A epoxy diacrylate (viscosity at 25°C = 27.1M g/(cm-s), M_w = 484.18), was purchased from Sartomer Co. (Exton, PA) and its chemical structure is shown in Figure 1. The radical photo-polymerization initiator, 1-hydroxycyclohexylphenyl ketone, was obtained from Chembridge International Co. (Taipei, Taiwan) Acrylic acid, tetraethyl orthosilicate (TEOS), anhydrous ethanol, isopropyl alcohol, and methanol to wash away the contaminants on glass substrates were purchased from Aldrich Chemicals (St. Louis, MO).

Synthesis of photo-curable polyacrylate/silica nanocomposites

Oligomer resins and TEOS were first mixed in a three-necked flask heated at 80°C. Appropriate amount of acrylic acid was then added dropwise into the oligomer/TEOS mixture. Instead of adding liquid water, the mixture was exposed to the atmospheric ambient at the relative humidity about 60% to acquire the moisture in ambient to hydrolyze the TEOS during the addition of acrylic acid. Previous process lasted about 2 h; a relatively small amount of water molecules entered into the system so that nano-scale silica particles could form in the resin samples. After that, the whole mixture was isolated from the ambient and continuously stirred for 24 h at 80°C to complete the sol-gel process. During the reaction, acrylic acid not only provided an acidic environment for the *in situ* sol-gel reaction, but also served as a reactive monomer for subsequent radical photo-polymerization. After the 24-h stirring, about 5.0 wt % photo-initiators were added into the mixtures and another 2-h stirring was carried to complete the preparation of nanocomposite resin samples. The content of photo-initiator in each of the samples was calculated as follows: (weight of initiators) ÷ [(weight of oligomer) + (weight of acrylic acid)] × 100%. The thin-film specimens were prepared by spin-coating the composite resins onto 76 × 26 × 1.3 mm^3 glass substrates followed by curing in an UV oven (CL-1000, UVP) in which the UV irradiation comes from an array of 8 W dual bipin discharge tubes emitting UV light in the wavelengths ranging from 350 to 400 nm (peak wavelength at about 365 to 370 nm) to induce the photo-polymerization. After UV curing, the films were all transparent and then post-cured at 80°C for 60 min.

Characterizations

IR and ^{13}C NMR analyses

Chemical structures of oligomer, acrylic acid, and resin samples were characterized by FTIR and NMR. The ^{13}C NMR spectra were obtained from a Varian UnityInova 500 NMR and $CDCl_3$ was used as the sample solvent. The FTIR spectra were obtained from a Nicolet Protégé 460 IR spectrometer.

Thermal analysis

DuPont 2950 thermogravimetric analyzer (TGA) was used to analyze the thermal properties and inorganic contents of composite samples. For the identifications of residual weight of inorganic content and 5.0% weight decomposition temperature, the samples were heated at a rate of 20°C/min from 30 to 900°C and then isothermally soaked for 5 min in air and N_2 atmospheres, respectively. The TGA data were also transformed to the derivative thermogravimetry (DTG) curves. In-plane thermomechanical analysis (TMA) was carried out in a DuPont 2940 TMA with micro-expansion probe at a heating rate of 5°C/min from 30 to 130°C to identify the coefficient of thermal expansion (CTE).

Microstructure analysis

The transmission electron microscopy (TEM) sample was prepared by spin-coating the composite resins onto KBr disc substrate. After the completion of cur-

TABLE I
Samples Prepared in this Work and Their Composition

Sample designation	Si[a] (wt %)	*F* factor[b]
Oligomer		
OA_1Si_5[c]	5.0 (19.81)[d]	1.0 (57.26/19.81)[e]
OA_1Si_{10}[c]	10.0 (22.35)[d]	1.0 (64.69/22.35)[e]
OA_1Si_{20}[c]	20.0 (23.80)[d]	1.0 (69.18/23.80)[e]
OA_2Si_{10}[c]	10.0 (19.80)[d]	2.0 (57.26/19.80)[e]
OA_4Si_{10}[c]	10.0 (12.59)[d]	4.0 (72.82/12.59)[e]
$OA_{0.25}Si_{10}$[c]	10.0 (43.45)[d]	0.25 (31.40/43.45)[e]
$OA_{0.25}Si_{20}$[c]	20.0 (49.70)[d]	0.25 (35.92/49.70)[e]

[a] The weight percentage of Si added per 100g of oligomer is measured according to

$$\frac{\text{molecular weight of Si}}{\text{molecular weight of TEOS}} \times \frac{\text{weight of TEOS}}{\text{weight of oligomers}} \times 100\%.$$

[b] The ratio of acrylic acid to TEOS is defined as the

$$F \text{ factor} = \frac{\text{weight of acrylic acid}}{\text{weight of TEOS}}.$$

[c] ''O'', ''Si,'' and ''A,'' respectively, represents the oligomer resin, TEOS, and acrylic acid. The subscript of Si represents the Si content while the subscript of A represents the value of *F* factor.

[d] The molar fraction of TEOS within oligomer/acrylic acid/TEOS mixture.

[e] The molar fraction of acrylic acid/TEOS within previous mixture.

ing, the KBr was then dissolved away in an acetone/DI water solution with the assistance of ultrasonic vibration to obtain the nanocomposite thin films. The thin films about 100 nm in thickness were then mounted on the carbon-coated copper (Cu) mesh and sent to a JEOL 2000FX TEM operating at 200 kV for microstructure characterization.

Other properties

The transmittance of nano-composite films was characterized by Hewlett–Packard UV-Visible 8453 spectrometer with scanning wavelengths ranging from 190 to 1200 nm. The moisture permeability was measured at 40°C and 90% RH using a permeation detection apparatus (PERMATRAN-W 3/60, MOCON) and the dimension of resin specimens is about $80 \times 80 \times 0.1$ mm^3. The size distributions of silica in composite resins were evaluated by a Honeywell UPA150 particle analyzer. Adhesion strengths of resin samples on glass substrates were measured in accordance with ASTM D-3528 standard.

RESULTS AND DISCUSSION

Synthesis of composite resins via sol-gel process and subsequent radical photo-polymerization

To characterize the influence of the moisture amount in sol-gel reaction, we defined the weight ratio of acrylic acid to TEOS as the *F* factor. Table I presents the composition of samples prepared in this work. Figure 2(a) shows the FTIR spectra of samples containing different weight percentages of Si in nanocomposite resins with *F* factor = 1 and Figure 2(b) shows the spectra difference of neighboring spectra in Figure 2(a). The —CH_2 peak at about 2950 cm^{-1} was assigned as the reference peak for comparison and differences higher than that were identified as the chemical variations. In Figure 2(a), the presence of —Si—O—Si— peak near 1090 cm^{-1} represents that the silica was indeed derived from TEOS via sol-gel reaction as reported by Landry et al.[15] Further, the spectra broaden as the content of Si increases from 5 to 10 wt %. However, as shown in Figure 2(b), there is no apparent broadening of —Si—O—Si— peak when Si content exceeds 20 wt % and similar phenomenon was also observed in the —Si—O—C— stretching band between 798 to 793 cm^{-1}.[20,21] It was also observed that

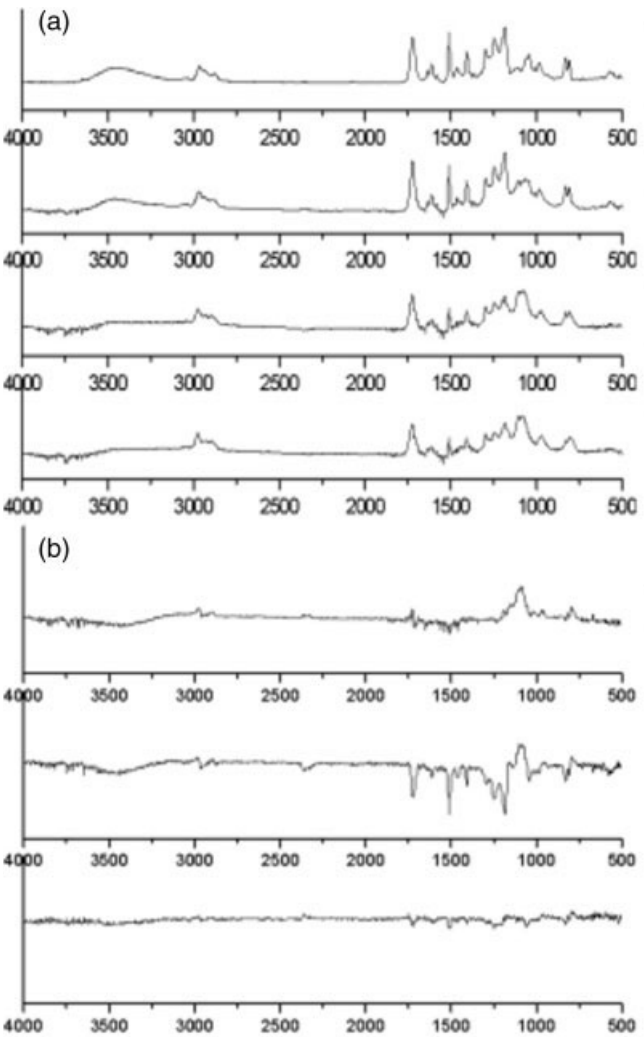

Figure 2 (a) FTIR spectra of the nanocomposite resin samples containing different Si wt % with fixed *F* factor (= 1); (b) difference of neighboring spectra shown in (a). The signs ''+''/''−'' represent the increase/decrease of absorbance of each functional group deduced from subtraction.

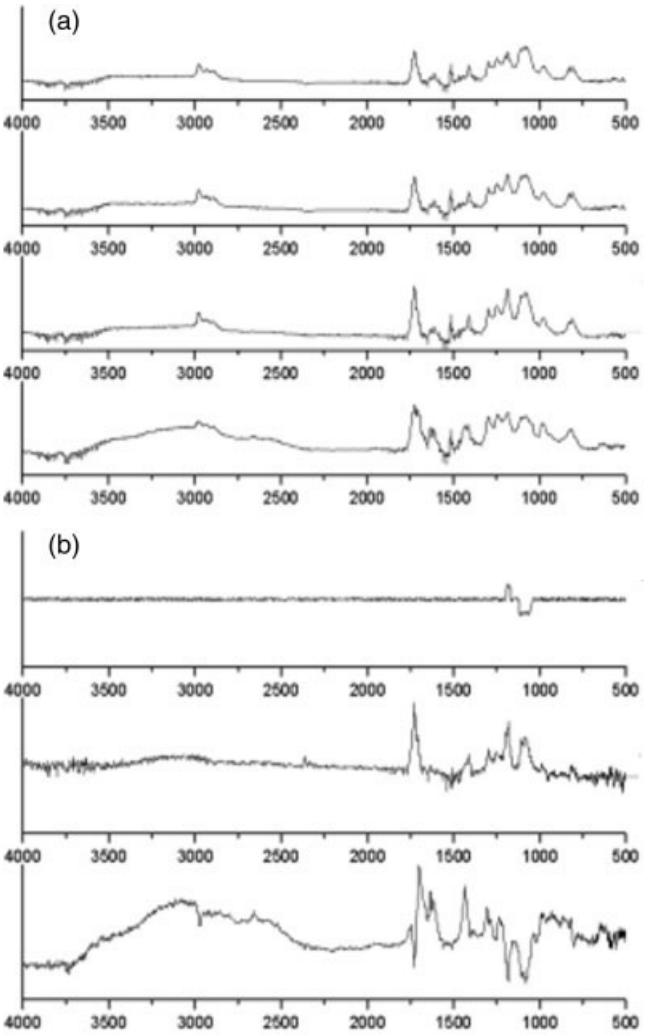

Figure 3 (a) FTIR spectra of the composite resin samples containing 10.0 wt % Si with different *F* factors; (b) difference of neighboring spectra shown in (a).

although the calculated molar fraction of acrylic acid increases from 57.26% to 69.18% with the increase of Si content, the broad hydroxyl group peak in alcohol, acid and —Si—OH[20,21] in between 3750 to 3300 cm^{-1}, gradually shrinks with the increase of Si content. These results evidence that the entire alkoxide groups of TEOS were not completely hydrolyzed into —OH groups and the silica formation was suppressed during the polycondensation stage. It also indicates that the organic molecular species containing —OH groups might undergo some other chemical reactions during sol-gel reaction.

Figure 3(a) shows the FTIR spectra of nanocomposite resins containing constant 10 wt % Si with *F* factor = 0.25, 1, 2, and 2, respectively, and Figure 3(b) shows the differential of neighboring spectra deduced from Figure 3(a). It was found that the sample with $F = 4$ exhibits an obvious decrease of —Si—O—Si— peak height in comparison with the spectra of the other three samples. Furthermore, no obvious —OH vibration band was observed in the spectra with *F* factors ≤ 2. However, an apparent positive variation of the shoulders among —C(=O)— peak between 1730 to 1710 cm^{-1}, generally caused by the existence of hydrogen bonds,[15] appeared in the differential spectra of OA_2Si_{10}—OA_1Si_{10} in comparison with that of OA_1Si_{10}-$OA_{0.25}Si_{10}$. As indicated by Figure 3(b), the sample with $F = 0.25$ comprises a larger —Si—O—Si— ($OA_{0.25}Si_{10} \approx OA_2Si_{10} > OA_1Si_{10} \approx OA_4Si_{10}$) and a smaller —OH signals ($OA_4Si_{10} > OA_2Si_{10} > OA_1Si_{10} > OA_{0.25}Si_{10}$). In typical silica sol-gel process, acid usually serves as the catalysts that hydrolyze the alkoxide to hydroxyl groups and the number of —Si—OH groups with respect to entire —Si—OEt groups was interrelated to subsequent polycondensation process. Hence, appropriate amount of water has to be added in proportion to the number of —Si—OEt groups to complete the hydrolysis. When the amount of water in the sol-gel process was limited, the suppression of —Si—O—Si— bonds was expected.

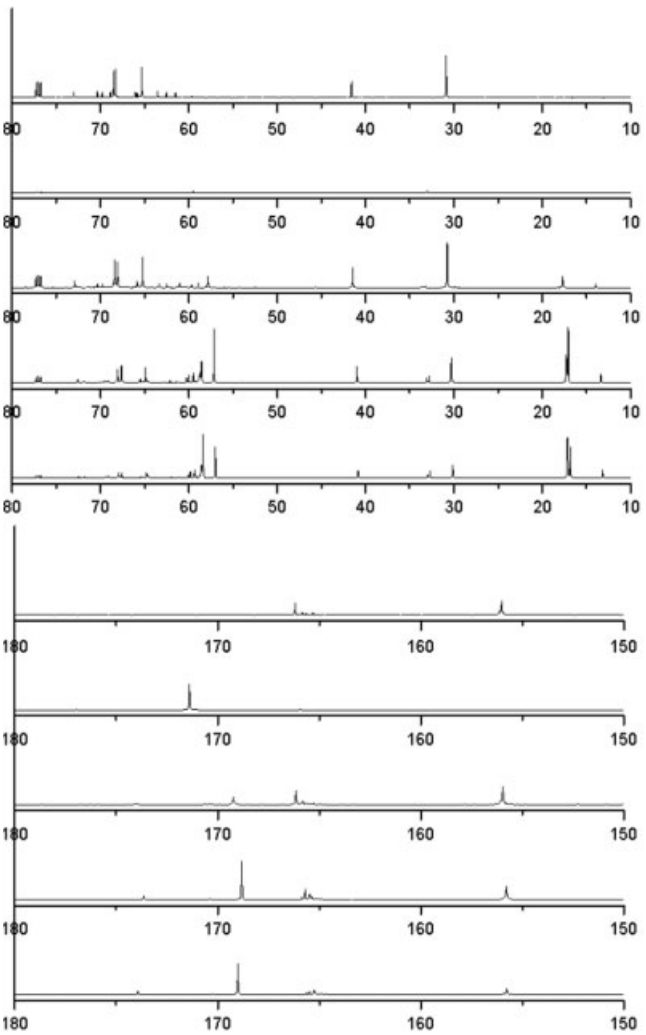

Figure 4 ^{13}C NMR spectra of composite resin samples containing different Si wt % with fixed *F* factor (= 1).

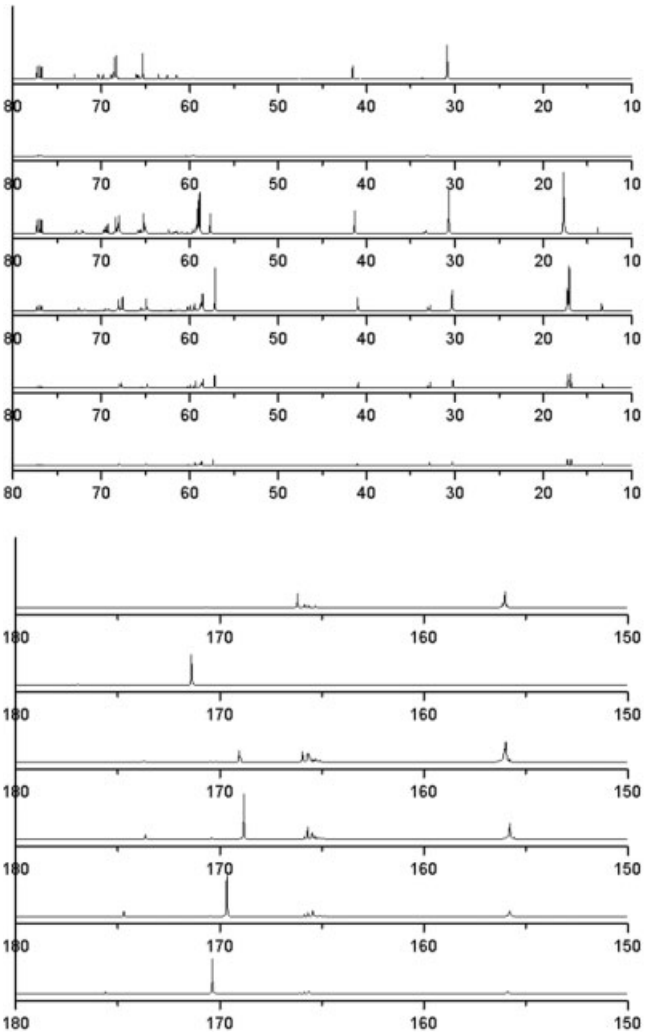

Figure 5 ^{13}C NMR spectra of the composite resin samples containing 10.0 wt % Si with different *F* factors.

Typically, the —OH signals in the FTIR spectra could be linked with the molar fraction (mf %) of acrylic acid/oligomer in the samples. Although OA_1Si_{10} contains 64.69 mf % of acrylic acid and 12.96 mf % of oligomer (calculated values), there is no clear information in whole OA_1Si_{10} spectra indicating the existence of —OH groups; hence the acrylic acid not only played as a catalyst, but also reacted with other ingredients at the condition of *F* factor ≤ 1 in the sol-gel process carried out in this study.

The ^{13}C NMR spectra of nanocomposite resins containing different weight percentages of Si with fixed *F* factor (= 1) are shown in Figure 4, while the NMR spectra of nanocomposite resins containing 10 wt % Si with different *F* factors are given in Figure 5. In all spectra, the gradual decline of peaks corresponding to oligomer evidences the decrease of molar fraction of oligomer in nanocomposite samples. In addition, there are new peaks observed in the chemical shift ranging from $\delta = 10$ to 65 ppm for all nanocomposite resin samples in comparison with the spectra of oligomer and acrylic acid. The new peaks localized at 17.6/57.0 ppm are originated from the two singlets —O—C—C*/—O—C*—C of ethanol,[22] and those at 13.5/58.5 ppm are associated with the —Si—O—C—C*/—Si—O—C*—C among ethoxy groups of TEOS. The —Si—O—C/—Si—O—C—C peaks correspond to the partial hydrolysis of TEOS inferred from previous FTIR analysis.

A comparison of chemical shifts for —O—C*—C groups in ethanol and —C(=O)— groups in acrylic acid are listed in Table II. The standard position of $CDCl_3$ is at 77.36 ppm while in our sample, it appears at 77.01 ppm. The chemical shift differences for specific carbon larger than ± 0.35 were hence attributed to the formation of new bonds. In Table II, the differences of chemical shift for —O—C*—C exceeds ± 0.35 were observed only in OA_1Si_5 and $OA_{0.25}Si_{10}$ and that for —C(=O)— was found in all resin samples. Generally, a downfield shift of C-1 next to a hydroxyl group indicated that the carbon within an electron-withdrawn group such as —C(=O)— is bonded to oxygen in —O—C— groups; moreover, the upfield shift of —C(=O)— indicated that an alkoxide or ester group is substituted for a hydroxyl group originally bonded to —C(=O)— groups. Therefore, an esterification induced by acrylic acid occurred in sample of $F = 0.25$ along with the sol-gel reaction. Another component necessary for esterification is the ethanol derived from sol-gel process, and new esters, such as ethyl acrylate, were hence generated. Since the upfield shift of —C(=O)— was observed in all samples, it was speculated that the new anhydrides, such as acrylic anhydride, form via condensation of acrylic acid in all samples.

During the sample preparation, we noted that the mixture became muddy when TEOS was added into oligomer. After adding acrylic acid dropwise into the oligomer/TEOS mixture and stirring for a certain period, the mixture turned into transparent. Because water for sol-gel process was acquired from the ambient, four —Si(OEt) groups in single TEOS molecule would be hydrolyzed by H_2O molecules randomly

TABLE II
Variation of 13C NMR Spectra Shown in Figures 3 and 4

Functional groups	Chemical shift (ppm)
HO—C*—C	
In free EtOH	57.0
In $OA_1Si_{5/10/20}$	+0.8/+0.1/0
In $OA_{0.25/1/2/4}Si_{10}$	+0.7/+0.1/+0.2/+0.3
—C=O	
In free acrylic acid	171.4
In $OA_1Si_{5/10/20}$	−2.2/−2.6/−2.4
In $OA_{0.25/1/2/4}Si_{10}$	−2.4/−2.6/−1.7/−1.0

"+" represents downfield shift and "−" represents upfield shift.

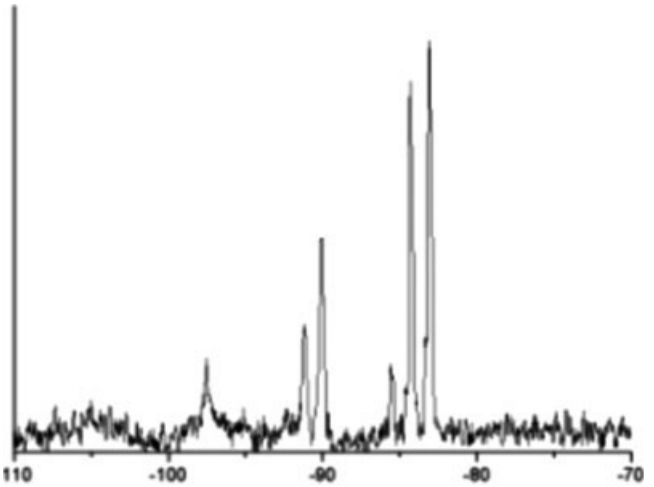

Figure 6 ^{29}Si-NMR spectrum of $OA_{0.25}Si_{10}$.

adsorbed on the ambient/mixture interface. The existence of $Si(OH)_x(OEt)_{4-x}$ transformed from TEOS was hence expected. Owing to the formation of hydrogen bonds between $Si(OH)_x(OEt)_{4-x}$/acrylic acids/oligomer during sol-gel process, the degree of phase separation between organic component and $Si(OH)_x(OEt)_{4-x}$ gradually reduced. Subsequently, $Si(OH)_x(OEt)_{4-x}$ molecules in the mixture polycondensed each other and formed silica particles cladding in —Si(OEt). The NMR was utilized to analyze the reactions stated above and the —Si—O—Si— structure derived by incomplete hydrolysis process. The ^{29}Si-NMR spectrum shown in Figure 6 evidenced the formation of —Si—O—Si— structure in $OA_{0.25}Si_{10}$. Referring to the —Si—O—Si— bonding status from ^{29}Si-NMR spectrum reported in previous study,[23] there is no free TEOS in $OA_{0.25}Si_{10}$. The signal peaks at −83.5 and −85.6 ppm correspond to the $—(SiO)Si(OEt)(OH)_2$ and $—(SiO)Si(OEt)_2(OH)$ structures, respectively; the $—(SiO)_2Si(OH)_2$ and $—(SiO)_2Si(OEt)(OH)$ were identified by the peaks at −90.1 and −91.2 ppm while the peak at −97.5 ppm was recognized as the formation of $—(SiO)_2Si(OEt)_2$. These results not only evidenced that the —Si—O—Si— structure in $OA_{0.25}Si_{10}$ was capped by organic functional groups, but also revealed the effects of moisture on the polycondensation of TEOS during sol-gel process. Although the consumption of —OH groups during the occurrence of polycondensation/esterification/

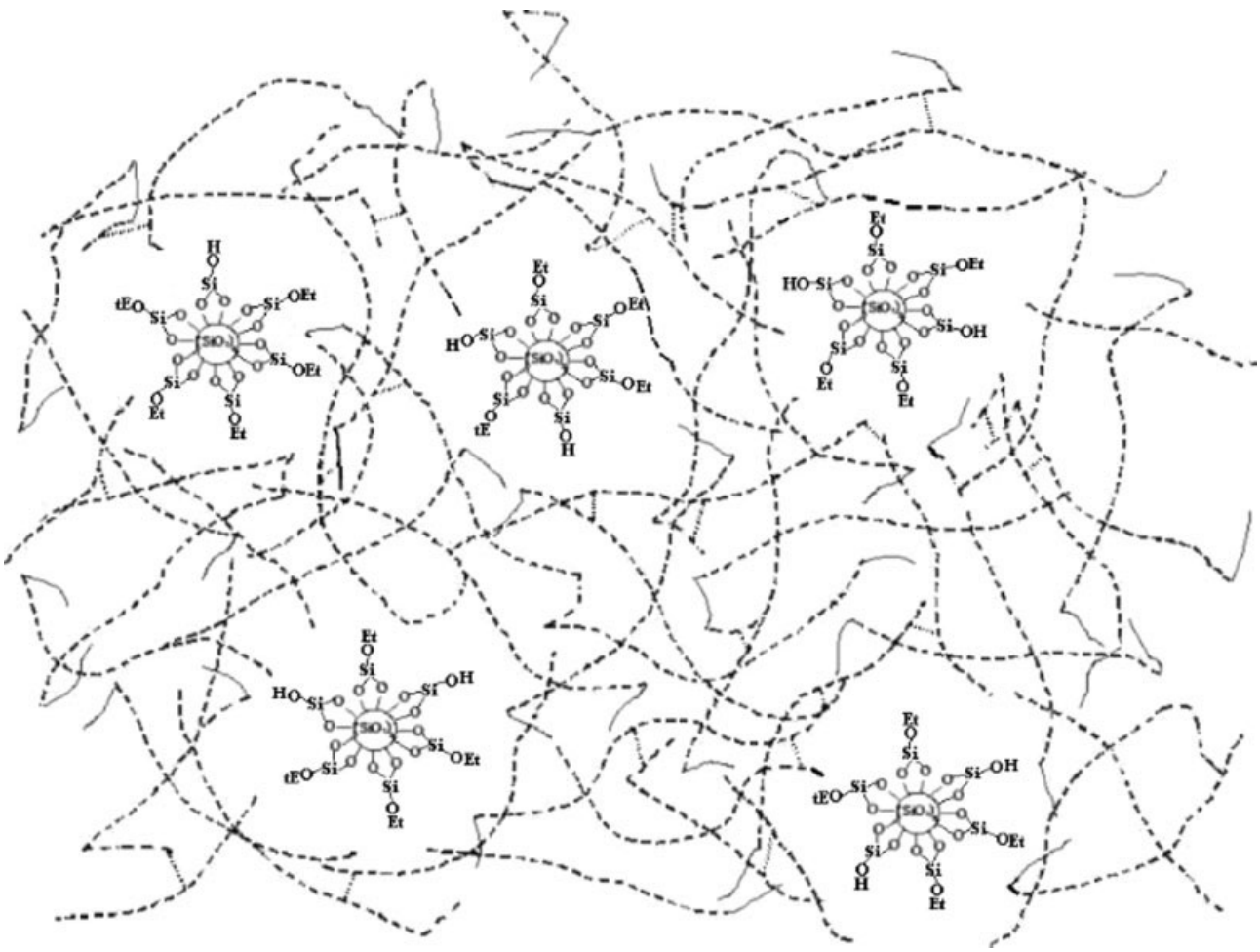

Figure 7 Schematic illustration of microstructure of nanocomposite resins prepared in this work.

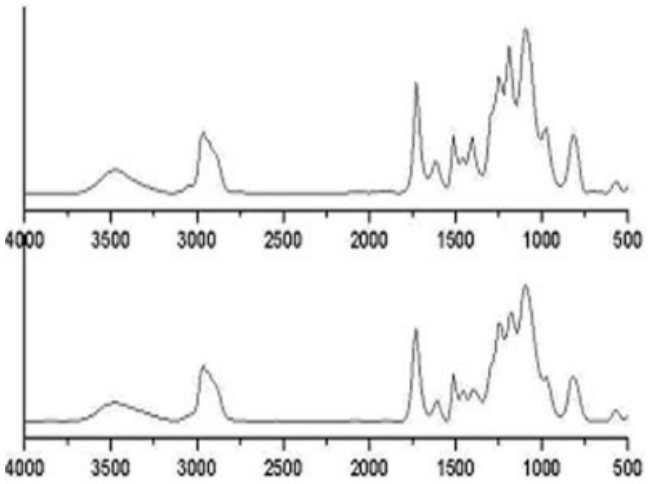

Figure 8 FTIR spectra of $OA_{0.25}Si_{10}$: (a) before and (b) after photo-polymerization.

condensation reduced the formation of hydrogen bonds, the degree of phase separation between organic component/silica particles did not occur due to the capping of —Si(OEt). Figure 7 schematically illustrates the microstructure of organic/inorganic phases in the nanocomposite resins.

During the sol-gel reaction with relatively small amount of water molecules, the nanocomposite resin comprising of acrylate functional groups was subsequently photo-polymerized when exposed to UV irradiation. It is known that the C=C double bonds among acrylate groups of oligomer/monomer will be broken by the radicals derived from the breakage of photo-initiators during UV exposure[24] and subsequently oligomer and monomer crosslink each other to complete the polymerization. Figure 8 shows the FTIR spectra of $OA_{0.25}Si_{10}$ before and after photo-polymerization. The $_2HC{=}C{-}$ stretching band of acrylate groups were identified around 1630 cm^{-1}. The reduction of $_2HC{=}C{-}$ peak in Figure 8 was clearly observed and the conversion ratio of $_2HC{=}C{-}$ in $OA_{0.25}Si_{10}$ calculated from the following formula was approximately equal to 41% while that of oligomer was about 78%. These results evidenced the occurrence of photo-polymerization during UV irradiation; however, the relatively low ratio was attributed to the intercalation of silica transformed from TEOS.[25]

$$\text{Conversion ratio}\,(\%) = \left(1 - \frac{\text{FTIR absorbance of } {}_2\text{HC}{=}\text{C after UV curing}}{\text{FTIR absorbance of } {}_2\text{HC}{=}\text{C before UV curing}}\right) \times 100.$$

Microstructure of nanocomposite thin films

The silica particle size distribution of $OA_{0.25}Si_{10}$ and TEM micrographs of $OA_{0.25}Si_{10}$ and $OA_{0.25}Si_{20}$ nanocomposite thin films are shown in Figure 9(a–c). The diameters of silica in $OA_{0.25}Si_{10}$ are in the range from 9.9 to 12.8 nm (99%) with average value equal to 11.5 nm, as indicated by the result of particle size

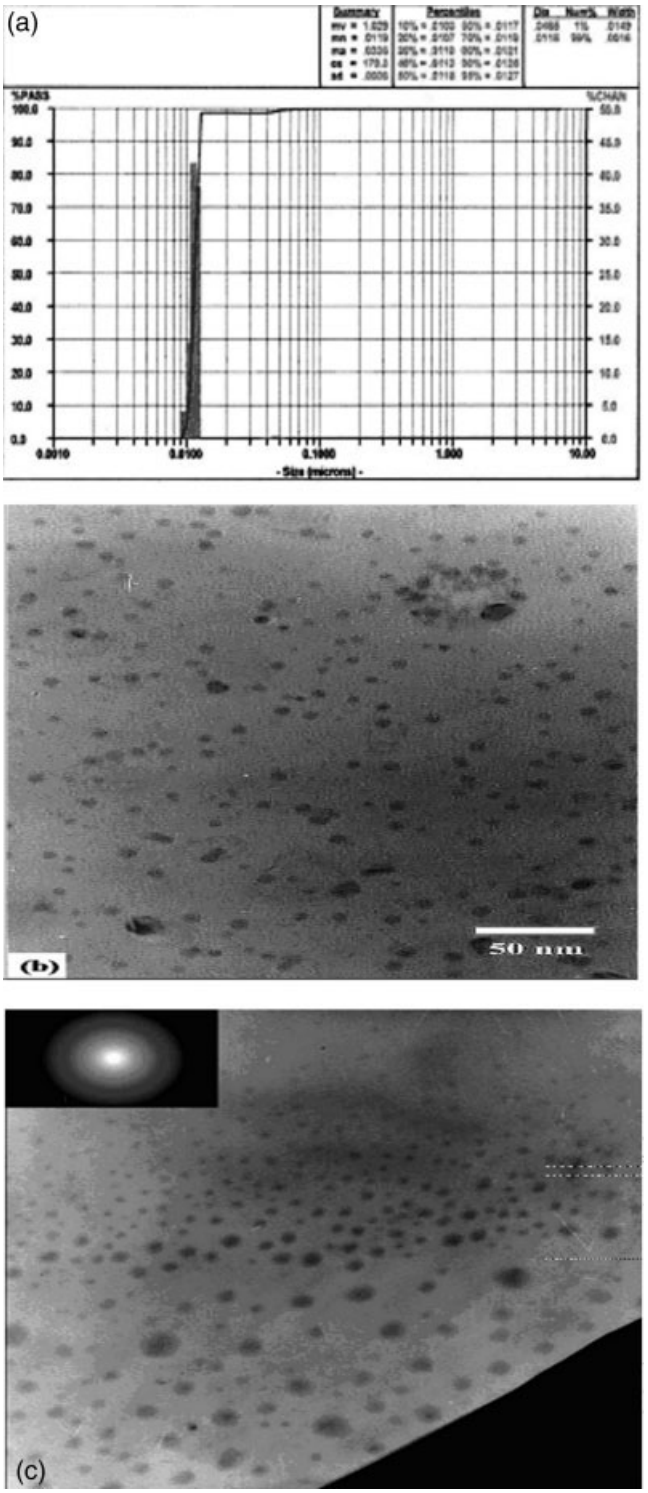

Figure 9 (a) Silica particle size distribution of $OA_{0.25}Si_{10}$ and (b) corresponding TEM micrograph. (c) TEM micrograph of $OA_{0.25}Si_{20}$ with selected area electron diffraction (SAED) pattern.

TABLE III
Thermal Properties of Oligomer and Nanocomposite Resins

	$T_{d-5\%}$ (°C)		$T_{d-50\%}$ (°C)		Residual
	In N_2	In air	In N_2	In air	weight (wt %)
Oligomer	367	342	468	459	–
$OA_{0.25}Si_{10}$	180	187	507	574	11.12
$OA_{0.25}Si_{20}$	154	158	497	589	15.72

analysis shown in Figure 9(a). The TEM observation for $OA_{0.25}Si_{10}$ not only confirmed the result of particle size analysis, it also revealed a uniform dispersion of silica particles in polymer matrix. In contrast to $OA_{0.25}Si_{10}$, the size of silica particles in $OA_{0.25}Si_{20}$ exhibits a wider distribution ranging from 20 to 100 nm although the distribution of silica particles remains uniform. Previous studies pointed out that the diameter of silica domain catalyzed by acid is much smaller than that catalyzed by base in sol-gel process,[16] and the intermolecular hydrogen bonds might enhance the compatibility between organic–inorganic phases.[26–29] With the NMR/FTIR analyses mentioned above, the clad —Si(OEt) resulted from partial hydrolysis of TEOS apparently benefited the size reduction and enhance the dispersion of silica particles in polymer matrix although hydroxyl groups might cap part of the silica particles. The conformational hindrance from molecular chains also restricted the growth of silica. Furthermore, the excess $Si(OH)_x(OEt)_{4-x}$ in $OA_{0.25}Si_{20}$ not only increased the number of nuclei for particle formation but also promoted the growth of silica particles. A wider distribution of nano-sized silica in $OA_{0.25}Si_{20}$ consequently obtained.

Thermal properties

Experimental results of TGA, DTG, TMA, and DMA analyses of oligomer, $OA_{0.25}Si_{10}$ and $OA_{0.25}Si_{20}$ are shown in Table III and Figure 10, respectively. The 5.0% weight loss decomposition temperature ($T_{d-5\%}$) of oligomer is about 367 °C in N_2 and 342 °C in air ambient while the 50% weight loss decomposition temperature ($T_{d-50\%}$) of oligomer reaches 468°C in N_2 and 458°C in air ambient. After the formation of nanocomposite resins, $T_{d-5\%}$ of samples decreases both in N_2 and air ambient with the increase of Si content and vice versa for $T_{d-50\%}$. As to the residual weight analysis, good consistence was observed in $OA_{0.25}Si_{10}$. However, in $OA_{0.25}Si_{20}$, the residual weight was only 15.72 wt %, which is lower than the theoretical value. As revealed by above analysis, this is resulted from the partial hydrolysis of TEOS by moisture in the ambient so that the —Si(OEt) did not completely transform into —Si(OH) during sol-gel process to form the silica particles. Incomplete hydrolysis of TEOS might affect the thermal stability of $OA_{0.25}Si_{20}$. As to the samples subjected to heat during TGA test, thermal prop-

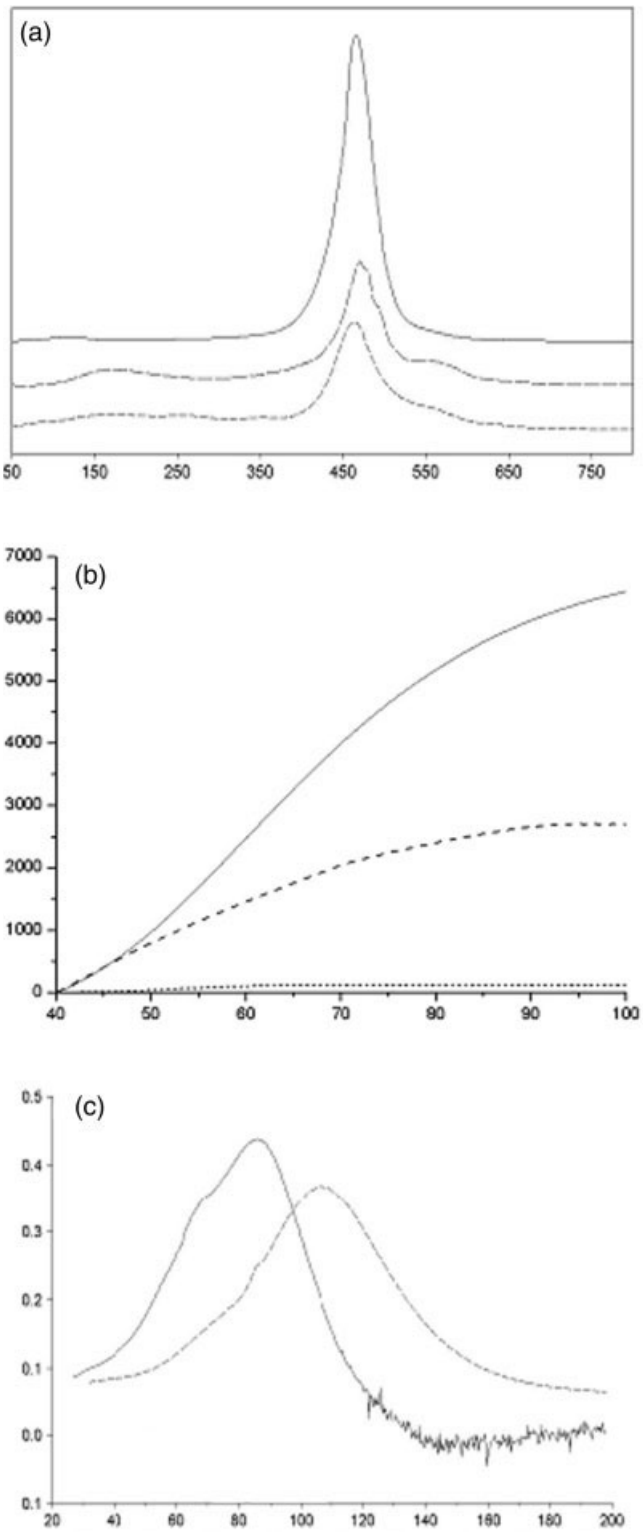

Figure 10 (a) DTG curves, (b) coefficient of thermal expansion (CTE) and (c) dissipation factors (tanδ) of (———) oligomer, (– –) $OA_{0.25}Si_{10}$, and (- - -) $OA_{0.25}Si_{20}$ deduced from DMA analysis. The dot lines in (a) represents the baseline in each curve and the numerals in (c) represent the glass transition temperature (T_g).

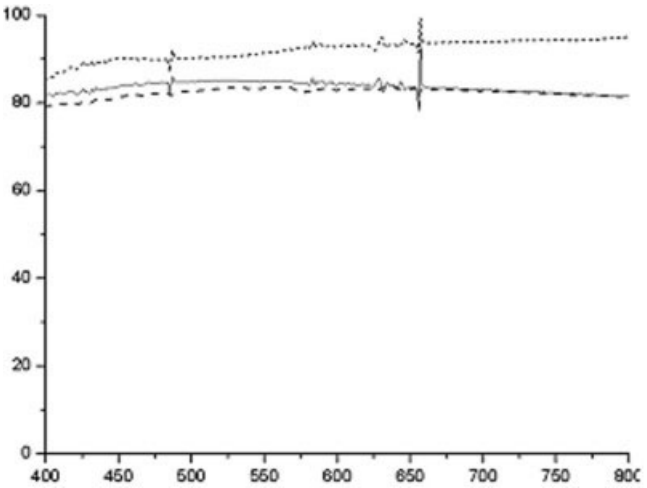

Figure 11 UV-Vis spectrum of (———) oligomer, (– –) $OA_{0.25}Si_{10}$ and (- - -) $OA_{0.25}Si_{20}$. The thickness of samples ≈ 100 μm.

erty change of nanocomposite films in comparison with that of oligomer could be more clearly seen when TGA data were transformed into the DTG curves shown in Figure 10(a). The information about intermolecular interactions and bonding formation could also be deduced from the plots of DTG curves. In Figure 10(a), there is a broad peak around 190°C for both nanocomposite resins. In addition to the major peak about 460°C, the peak ''shoulder'' also appears around 570°C for $OA_{0.25}Si_{10}$ and $OA_{0.25}Si_{20}$. Since we adopted sol-gel process for sample preparation, short-chain segments in *co*-polyacrylate backbone derived from photo-polymerization between oligomer and small molecules might decompose at the early stage of heating.[29,30] Another explanation for this phenomenon proposed by Huang and Qui[28] and Ma and coworkers[31,32] is that the intermolecular hydrogen bonds might form via the —OH groups of $(SiO_2)_x$ and carbonyl groups of PMMA in the case of PMMA/SiO_2 hybrids prepared by sol-gel process. In this study, although previous FTIR analysis indicated that a few free —OH exists in nanocomposite resins, the peak around 190°C should still attribute to the possible breakage of interchains hydrogen bonds. The peak around 460°C corresponds to the decomposition of photo-polymerized oligomer. Owing to two 2°—OH groups within oligomer, acrylic acid might also react with them to esterify the oligomer even if it is generally understood that 2°—OH is less reactive than 1°—OH.[22] The ''shoulder'' of DTG peak hence correlated to the decomposition of esterified oligomer. TMA analysis shown in Figure 10(b) revealed that the CTE of the samples decreases from 99.2 ppm/°C for pure oligomer, to 30.6 ppm/°C for $OA_{0.25}Si_{10}$ and to 22.7 ppm/°C for $OA_{0.25}Si_{20}$. Organic materials usually possess higher CTE values than those of the inorganic. This implies that the formation of silica in polymer is able to reduce of the CTE of organic–inorganic composites. Interlaced nano-sized silica particles hence reduce the volume expansion of polymer network in polymer/silica composites. As shown in Figure 10(c), the dissipation factor (tanδ) deduced from DMA analysis indicates that $OA_{0.25}Si_{10}$ possesses less dissipation in comparison with oligomer and the glass transition temperature (T_g) of $OA_{0.25}Si_{10}$ ($\sim$ 107°C) is higher than that of oligomer ($\sim$ 86°C). Hu et al. reported that cladding of organic groups on nano-sized particles restricts the mobility of polymer chains because polymer chains were tethered to the organic portion.[33] Owing to the existence of uniformly dispersed nano-silica particles capped with —O—CH_2CH_3 and —OH groups in polymeric matrix, it is apparent that the frictions between polymer chains and —O—CH_2CH_3/—OH groups capped on silica particles effectively restrict the mobility of *co*-polyacrylate chains so as to form a more rigid structure. The nanocomposite samples hence possessed smaller dissipation factor and higher T_g.

Other properties

After photo-curing and post baking, all samples retained good transparency. The transmittance in the wavelength range of visible light is shown in Figure 11. Our calculation showed that the average transmittances between 400 to 800 nm are 82.33%, 81.92%, and 89.61% for oligomer, $OA_{0.25}Si_{10}$, and $OA_{0.25}Si_{20}$, respectively. Since the sizes of silica are in nanometer scale, the degree of light scattering is reduced so that there is no severe deterioration of transmittance of the nanocomposite samples.

Experimental results of moisture absorption listed in Table IV show that the $OA_{0.25}Si_{10}$/$OA_{0.25}Si_{20}$ absorbs less moisture in comparison with oligomer. The results of moisture permeability measurement further confirmed that the nanocomposite sample possesses higher resistance to moisture penetration. It is believed that the finely dispersive, nano-scale silica in polymer may effectively serve as a barrier to moisture diffusion so as to suppress the moisture permeability of nanocomposite materials.

TABLE IV
Moisture Absorption, Moisture Permeability, and Adhesion Strengths of Oligomer and Nanocomposite Resins

	Moisture absorption (%)	Moisture permeability[a] ($g/m^2 \cdot 24$ h)	Adhesion strength (kgf/cm^2)
Oligomer	1.15	13.59	20.23
$OA_{0.25}Si_{10}$	1.01	10.41	42.76
$OA_{0.25}Si_{20}$	1.07	–	102.27

[a] The amount of moisture penetrating through resin film sample in 24 h.

Adhesion test results shown in Table IV indicate that the adhesion strengths of $OA_{0.25}Si_{10}$ and $OA_{0.25}Si_{20}$ are higher than that of oligomer. For examples, the adhesion strengths of $OA_{0.25}Si_{10}$ and $OA_{0.25}Si_{20}$ are two- and five-folds higher than that of oligomer, respectively. It is known that the hydrogen bonds formed at the nanocomposite-glass interface might enhance the adhesion strength.[32] In nanocomposite resin samples, both free —OH groups and carbonyl groups in polyacrylate backbone form hydrogen bonds with —OH groups on glass substrates to improve adhesion strength; moreover, nano-sized silica particles clad in ethoxy did not suppress the adhesion strength. Hence the enhancement of adhesion property was observed.

CONCLUSIONS

Photo-curable *co*-polyacrylate/silica nanocomposites were prepared via sol-gel process. The FTIR and ^{13}C NMR analyses indicated that segmental esters and anhydride were formed in $OA_{0.25}Si_{10}$/$OA_{0.25}Si_{20}$ nanocomposite resin samples along with the sol-gel process, and the inorganic silica cladded in ethoxy groups. During UV exposure, the C=C double bonds among acrylate groups were broken by radicals derived from photoinitiators to complete the formation of nanocomposite films via photo-polymerization. TEM observation revealed that the silica particles with average sizes 11.5 nm were uniformly distributed in the polymer matrix for $OA_{0.25}Si_{10}$ sample. In $OA_{0.25}Si_{20}$, which contained higher Si wt %, nano-scale silica particles with wider size distribution were observed. Such fine particle dispersions were attributed to the formation of interchain hydrogen bonds and/or the compatible ethoxy groups in the surrounding of silica resulted from the partial hydrolysis of TEOS. The TGA/DTG analysis showed that the thermal stability of $OA_{0.25}Si_{10}$ and $OA_{0.25}Si_{20}$ decreases due to the breakage of hydrogen bonds and newly formed short segments. The thermal analysis also implied the formation and crosslinking of esterified oligomers via photo-polymerization. Depends on the Si content, addition of silica effectively reduced the CTE's of the composites up to one-third of the value of oligomer. Other property characterizations indicated that the *co*-polyacrylate/silica composites possessed satisfactory transmittance above 80% in visible light region and lower moisture absorption/permeability. This evidenced that, in addition to serve as an effective moisture permeation barrier, the nano-scale silica particles did not cause severe light scattering and hence could be applied to direct encapsulation of optoelectronic devices such as OLEDs. Adhesion tests indicated that —OH and carbonyl groups in polyacrylate backbone might form hydrogen bonds with the —OH groups on the surface of glass substrate so a substantial improvement of adhesion strength was achieved.

References

1. Popovic, Z. D.; Xie, S.; Hu, N.; Hor, A.; Fork, D.; Anderson, G.; Tripp, C. Thin Solid Film 2000, 363, 6.
2. Tak, Y. H.; Kim, K. B.; Park, H. G.; Lee, K. H.; Lee, J. R. Thin Solid Film 2002, 411, 12.
3. Jeong, Y. S.; Ratier, B.; Moliton, A.; Guyard, L. Synth Met 2002, 127, 189.
4. Kim, G. H.; Oh, J.; Yang, Y. S.; Do, L. M.; Suh, K. S. Polymer 2004, 45, 1879.
5. Liu, T.; Lim, K. P.; Tjin, W. C.; Pramoda, K. P.; Chen, Z. K. Polymer 2003, 44, 3529.
6. Huang, J. C.; He, C. B.; Xiao, Y.; Mya, K. Y.; Dai, J; Siow, Y. P. Polymer 2003, 44, 4491.
7. Zimmerman, A. F.; Palumbo, G.; Aust, K. T.; Erb, U. Mater Sci Eng A 2002, 328, 137.
8. Isik, I.; Yilmazer, U.; Bayram, G. Polymer 2003, 44, 6371.
9. Messersmith, P. B.; Giannelis, E. P. Chem Mater 1994, 6, 1719.
10. Pereira, A. P. V.; Vasconcelos, W. L.; Oréfice, R. L. J Non-Cryst Solid 2000, 273, 180.
11. Motomatsu, M.; Takahashi, T.; Nie, H. Y.; Mizutani, W.; Tokumoto, H. Polymer 1997, 38, 177.
12. Ghosh, N. N.; Pramanik, P. NanoStruc Mater 1997, 8, 1041.
13. Brinker, C. J.; Scherer, W. G. Sol-Gel Science/the Physics and Chemistry of Sol-Gel Processing, Chapter 3; 1990.
14. Oh, E. O.; Chakrabarti, K.; Jung, H. Y.; Whang, C. M. Mater Sci Eng B 2002, 90, 60.
15. Landry, C. J. T.; Coltrain, B. K.; Wesson, J. A.; Zumbulyadis, N.; Lippert, J. L. Polymer 1992, 33, 1496.
16. Landry, C. J. T.; Coltrain, B. K.; Brady, B. K. Polymer 1992, 33, 1486.
17. Nagata, H.; Shiroshi, M.; Miyama, Y.; Mitsugi, N.; Miyamoyo, N. Opt Fiber Technol 1995, 1, 283.
18. Baikerikar, K. K.; Scranton, A. B. Polymer 2001, 42, 431.
19. Wang, Y. Y.; Hsieh, T.-E.; Chen, I. C.; Chen, C. H. IEEE Trans Adv Packaging, to appear.
20. Innocenzi, P. J Non-Cryst Solids 2003, 316, 309.
21. Méndez-Vivar, J.; Mendoza-Bandala, A. J Non-Cryst Solids 2000, 261, 127.
22. Silverstein, R. M.; Bassler, G. C.; Morrill, T. C. Spectrometric Identification of Organic Compounds, 5th ed.; Wiley: New York, 1991.
23. Hook, R. J. J Non-Cryst Solids 1996, 195, 1.
24. Decker, C.; Nguyen Thi Viet, T.; Decker, E.; Weber-Koehl, E. Polymer 2001, 42, 5531.
25. Salmi, A.; Benfarhi, S.; Donnet, J. B.; Decker, C. Eur Polym J 2006, 42, 1966.
26. Stevens, N. S. M.; Rezac, M. E. Polymer 1999, 40, 4289.
27. Ha, C. S.; Park, H. D.; Frank, C. W. Chem Mater 2000, 12, 839.
28. Huang, Z. H.; Qiu, K. Y. Polymer 1997, 38, 521.
29. Salahuddin, N.; Shehata, M. Polymer 2001, 42, 8379.
30. Xu, M.; Choi, Y. S.; Kim, Y. K.; Wang, K. H.; Chung, I. J. Polymer 2003, 44, 6397.
31. Chiang, C. L.; Ma, C. C. Eur Polym J 2002, 38, 2219.
32. Chiang, C. L.; Yih, F. Y.; Ma, C. C.; Chang, H. R. Polym Degrad Stab 2002, 77, 273.
33. Hu, Y. H.; Chen, C. Y.; Wang, C. C. Polym Degrad Stab 2004, 84, 545.